

Angle-resolved photoelectron spectroscopy and band-structure calculations of CdI_2

R. Coehoorn, G. A. Sawatzky, and C. Haas

*Laboratories of Physical and Inorganic Chemistry, Materials Science Centre of the University of Groningen,
Nijenborgh 16, 9747 AG Groningen, The Netherlands*

R. A. de Groot

*Research Institute for Materials, Faculty of Science, University of Nijmegen, Toernooiveld,
6525 ED Nijmegen, The Netherlands*

(Received 27 November 1984)

The electronic structure of the $4H$ polytype of the layered compound CdI_2 was investigated using angle-resolved ultraviolet photoelectron spectroscopy (ARUPS). The spectra are compared with results of self-consistent relativistic band-structure calculations of the $2H$ - and $4H$ - CdI_2 polytypes. It is shown that a detailed analysis of the spectra is possible by using calculated band dispersions. The calculated band structures are compared with the complete spectra and not only to the peak positions. The spectra can be explained by assuming indirect transitions. The wave-function symmetries were determined from the variation of peak intensities with the photon angle of incidence. The agreement between the calculated band structure and the experimental spectra is good; no significant differences between the calculated valence-band structure and the ARUPS spectra in excess of 0.3 eV are found.

I. INTRODUCTION

The electronic structure of many layered compounds has been studied successfully by angle-resolved ultraviolet photoelectron spectroscopy (ARUPS). In the photoemission process k_{\perp} , the component of the wave vector normal to the surface is not conserved, and measurements on one crystal surface using only a single photon energy generally do not give sufficient information for the construction of an experimental band structure, or for a critical test of calculated band structures. On performing ARUPS experiments on layered compounds such as graphite,^{1,2} InSe ,³ GaS ,⁴ and GaSe ,⁴⁻⁸ advantage has been taken of the relatively small energy dispersion in a direction perpendicular to the surface of certain electron states in the valence band. ARUPS spectra give direct information about the band structure in this case.

The dihalides and dichalcogenides of many transition metals and some post-transition metals (Sn, Pb, Cd) form another class of layered compounds. Each layer consists of three sublayers in the order X - T - X , where T is the transition-metal atom and X is the nonmetal atom. As far as the metal-derived d states are concerned, the band structure of these compounds is quasi-two-dimensional. The large interlayer metal-metal distance (5 Å or more) leads to a small dispersion of these states in a direction perpendicular to the layers (typically 0.1–1 eV). The presence of these states at the Fermi level can lead to the formation of two-dimensional charge-density waves.^{9,10} However, the electronic structure is three dimensional as far as the nonmetal p states in the valence band are concerned, because the interlayer distances between the nonmetal atoms are equal to their intralayer distances. This can lead to serious difficulties in the interpretation of ARUPS spectra of these layered compounds, even if a cal-

ulation of the band structure is available. Closely connected to this problem is the question of which theoretical model for the photoemission from this class of layered compounds has to be used: a direct transition model in which k_{\perp} is conserved during the optical transition, or an indirect transition model in which k_{\perp} is completely undetermined, leading to a spectrum which resembles a one-dimensional density of states (ODDOS).

From an analysis of ARUPS spectra not only information about the bulk band structure and the photoemission process can be obtained. For TaS_2 , for example, it was reported that ARUPS spectra as a function of temperature contain evidence of a Mott-Anderson metal-insulator transition.¹¹ In TiTe_2 a dispersionless state just below the Fermi level was ascribed to polaronic effects.¹² ARUPS has also been performed on intercalates of TiSe_2 with V.¹³ In all these cases it is important to be able to separate bulk band-structure effects from many-particle effects or effects of intercalated atoms. For this purpose a reliable band structure of the solid is required. In order to check the validity of the one-electron approximation as in calculated band structures a detailed comparison with ARUPS is needed.

In this paper we will show how results of band-structure calculations can be used to analyze the ARUPS spectra of CdI_2 (a layered insulating compound) in more detail than is usually done. The spectra were measured at a single photon energy (He I) with a high energy and angular resolution. These new experimental data complement and extend the work of McCannan *et al.*,¹⁴ who performed ARUPS measurements and band-structure calculations of CdI_2 . We compare our experimental data with the results of *ab initio* band-structure calculations of two polytypes: $2H$ - CdI_2 and $4H$ - CdI_2 . This latter polytype was used for the ARUPS measurements and has been reported to be

the most stable polytype.¹⁵ The calculations are expected to be important improvements of previous calculations of the band structure of $2H\text{-CdI}_2$.^{14,16,17} The present calculations are self-consistent, are based on a larger basis set of valence orbitals, and relativistic effects including spin-orbit interaction have been taken into account. The comparison between theory and experiment is based on calculations of the band structure along lines of constant k_{\parallel} in the emission planes. The experimental spectra were transformed to spectra at constant k_{\parallel} , and compared to the band structures. In this way more details in the spectra can be used for a comparison of theory and experiment than if a band structure from the literature, which only gives the dispersion along lines of high symmetry, is used. In the case of CdI_2 the analysis shows that the spectra can be interpreted using the indirect transition model. Attention is paid to the question of whether the $2H$ or the $4H$ band structure provides the best interpretation of the spectra.

We will restrict the discussion of the electronic structure of CdI_2 to the occupied states. An analysis of optical reflection spectra between 2 and 0 eV in terms of the band-structure calculation presented here, will be given by Thomas *et al.*¹⁸ Optical studies of CdI_2 have been reported by many authors, using different techniques. We will not give an exhaustive survey of this literature, but rather mention a few papers that can be used as an entry to other work. Reflection spectra have been reported by Greenaway and Harbeke,¹⁹ Matsumoto *et al.*,²⁰ and Bordas *et al.*¹⁶ Photoconductivity experiments have been performed by Yu²¹ and Wright and Tubbs.²² Luminescence spectra were reported by Hayashi *et al.*²³ Brothers and Pajor²⁴ studied the temperature and pressure dependence of the exciton spectra. Electron-energy-loss spectroscopy was performed by Bringans and Liang.²⁵

In Secs. II and III we describe the crystal structures and give some experimental details. In Sec. IV band-structure calculations of $2H$ - and $4H\text{-CdI}_2$ are presented. In Sec. V the theory of ARUPS is discussed, and the experimental results are presented. The spectra are compared with the calculated band structure. The peak intensities of the normal emission spectra as a function of the photon energy are shown to give information about the wave-function symmetries. This section also contains a discussion of the spin-orbit splitting of the $\text{Cd } 4d$ band in Cd metal and Cd compounds. Section VI contains some concluding remarks.

II. CRYSTAL STRUCTURES

Because of the weak binding between the layers, the total free enthalpy differences between CdI_2 compounds with different stackings of the layers is very small. Over 160 stacking sequences (polytypes) have been observed for CdI_2 .²⁶ The $4H\text{-CdI}_2$ structure, which consists of four anion layers, has been reported to be the most stable polytype.¹⁵ All other polytypes eventually transform to the $4H$ structure on heating. The most simple polytype consists of only two anion layers. This $2H$ structure and the $4H$ structure both have hexagonal unit cells [Fig. 1(a)]. The (110) cross sections of the unit cells are shown in Fig.

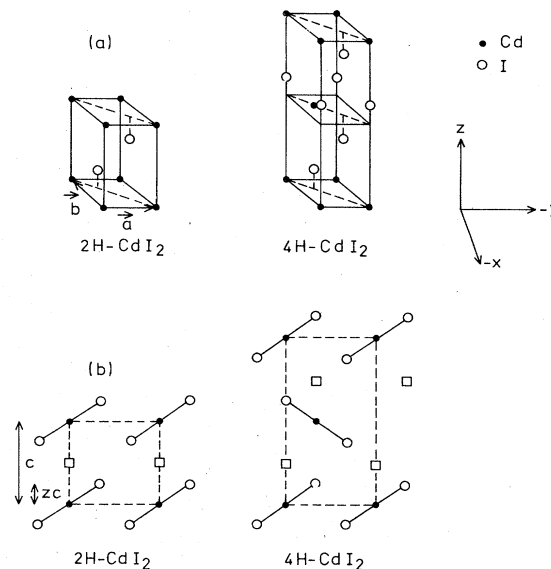


FIG. 1. (a) Hexagonal unit cell of $2H$ and $4H\text{-CdI}_2$. (b) (110) cross sections of the unit cells of $2H$ - and $4H\text{-CdI}_2$. The squares are vacant octahedral sites in the van der Waals gap.

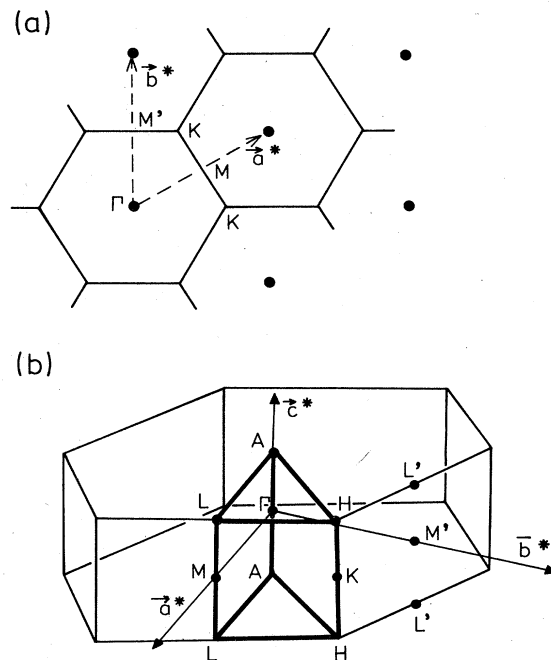


FIG. 2. (a) Reciprocal lattice of the CdI_2 structure in the a^*-b^* plane. The Brillouin zone is shown in the repeated zone representation. (b) Brillouin zone of the $2H$ - and $4H\text{-CdI}_2$ structure. For the $4H$ structure the plane $\Gamma ALM'$ is equivalent to the ΓALM plane. The $\frac{1}{12}$ irreducible part of the zone (for both structures) is shown by bold lines. The lines and planes of high symmetry have the following labels: ΓA , Δ ; ΓK , T ; ΓM , Σ ; AH , S ; ΓALM , F ; KM , T' ; AL , R ; HL , S' . ΓAHK , which is only for the $4H\text{-CdI}_2$ structure a high-symmetry plane, is called B .

1(b). In this figure the squares indicate vacant octahedral sites in the van der Waals gap.

The $2H$ structure has the symmorphic space group $P\bar{3}m1-D_{3d}^3$. The hexagonal unit cell consists of a Cd atom at the $1a$ site $(0,0,0)$ and two I atoms at the $2d$ sites $(\frac{1}{3}a\sqrt{3}, 0, zc)$ and $(\frac{1}{6}a\sqrt{3}, -\frac{1}{2}a, (1-z)c)$ in a Cartesian frame (x, y, z) . The experimental lattice parameters at 300 K are²⁷ $a=4.24$ Å, $c=6.84$ Å. The parameter z shows no measurable deviation from the ideal value $z=0.25$. As the c/a ratio deviates from the "ideal" value $c/a=\sqrt{8/3}$, for which the I atom would form a hexagonal close-packed structure, the Cd atoms are coordinated by a slightly trigonally distorted octahedron of I atoms. The octahedral hole in the gap at the $1b$ site has the position $(0,0,\frac{1}{2}c)$.

The $4H$ structure has the nonsymmorphic space group $P6_3mc-C_{6h}^4$. The unit cell consists of Cd atoms at $2b$ sites $(0,0,0)$ and $(\frac{1}{3}a\sqrt{3}, 0, \frac{1}{2}c)$, I atoms at $2b$ sites $(0,0,\frac{5}{8}c)$ and $(\frac{1}{3}a\sqrt{3}, 0, \frac{1}{8}c)$, and I atoms at $2a$ sites $(\frac{1}{6}a\sqrt{3}, -\frac{1}{2}a, \frac{3}{8}c)$ and $(\frac{1}{6}a\sqrt{3}, -\frac{1}{2}a, \frac{7}{8}c)$ in a Cartesian frame. Here the z parameter has been given its experimental values $z=\frac{1}{8}$. The coordinates of the vacant octahedral sites in the gaps at $2b$ sites are $(0,0,\frac{1}{4})$ and $(\frac{1}{3}a\sqrt{3}, 0, \frac{3}{4})$.

The Brillouin zone of the $2H$ [shown in Fig. 2(b)] and $4H$ polytypes have the same symmetry. The Brillouin zone of $4H$ -CdI₂ has half the height along the c^* direction. The reciprocal lattice in the a^*-b^* plane is shown in Fig. 2(a). For the $2H$ structure the ΓALM and $\Gamma AL'M'$ planes are inequivalent as the crystal symmetry is trigonal. This distinction does not occur for the $4H$ structure, which has hexagonal symmetry.

III. EXPERIMENTAL

Single crystals of CdI₂ were obtained from the melt by the Bridgman technique. The crystal structure and orientation were determined by Laue x-ray back reflection with unfiltered Mo $K\alpha, \beta$ radiation, using the intensities of the diffraction spots, which were compared with calculated intensities for $2H$ and $4H$ structures. The peak positions, calculated with the known unit-cell constants, and the peak intensities were in good agreement with the $4H$ structure. In particular, it was observed that the diffraction spectrum had sixfold symmetry, whereas the spectrum of $2H$ -CdI₂ is expected to have threefold symmetry.

ARUPS experiments were performed using a Vacuum Generators, ADES 400 spectrometer. A fresh surface was obtained by stripping the crystal with the use of adhesive tape. This was done in the preparation chamber, at a pressure of 10^{-7} Pa. The sample was transferred immediately to the main chamber, where the base pressure was lower than 10^{-8} Pa. The radiation source was a helium-gas discharge lamp, supplying unpolarized photons of 21.2 eV (He I) and of 40.8 eV (He II). A hemispherical analyzer was used at a constant pass energy of 5 eV. The energy resolution (0.1 eV) was 2% of the pass energy (5 eV). The acceptance angle was $\pm 1^\circ$.

Unfortunately the He II valence-band spectrum coincides in energy with the Cd $4d$ spectrum from the He II satellite line at $h\nu=48.37$ eV. The main-line to satellite-

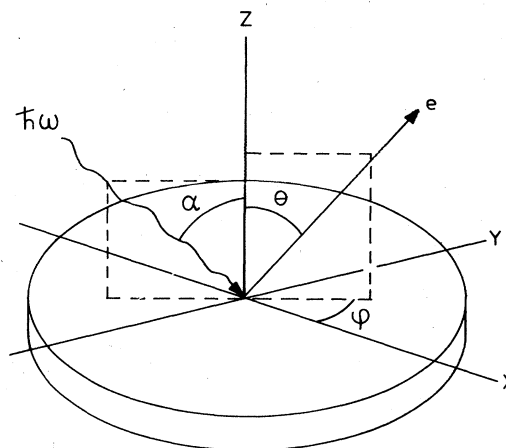


FIG. 3. Experimental geometry for angle-resolved photoemission. The photon plane of incidence is the same as the electron emission plane. This electron emission plane can be selected by rotating the crystal over an angle ϕ around the normal on the surface.

line intensity ratio was small (about 5:1 at the He pressure of 3.1 Pa in the gas discharge lamp) but the cross-section ratio of Cd $4d$ and I $5p$ states at these photon energies is very unfavorable (also about 5:1). Since the satellite line dominated the He II valence-band spectra, we will not discuss them.

The emitted photoelectrons were detected in the plane of the surface normal and the incoming photon beam. In Fig. 3 the angle of incidence of the light α and the emission angle of the photoelectrons θ are defined.

Charging of the samples during the photoemission experiment was prevented by heating the samples to 100–125°C. The same procedure was used by McCann *et al.*¹⁴ Conductivity measurements showed an enhancement of the conductivity by a factor of 100 on heating from 25 to 150°C. This effect is probably due to increased ionization of states in the gap, due to impurity atoms or Frenkel disorder of the Cd atoms. A fresh surface could be obtained by heating the crystal several minutes to about 200°C. The spectra which were measured after stripping the samples were the same as those which were measured after this heat treatment. We assume that by this treatment some layers at the surface of the sample are evaporated, including the contaminating atoms.

IV. BAND-STRUCTURE CALCULATIONS

A. Computational details

Self-consistent band-structure calculations of $2H$ -CdI₂ and $4H$ -CdI₂ were performed using the augmented-spherical-wave (ASW) method of Williams, Kübler, and Gelatt.²⁸ Exchange and correlation were treated within the local-density approximation, as given by Hedin and Lundqvist.²⁹ Scalar relativistic effects (mass velocity and Darwin terms)³⁰ and spin-orbit interaction were included

in the calculation. An atomic spin-orbit Hamiltonian of the form

$$\lambda \mathbf{L} \cdot \mathbf{S} = \lambda \left[\frac{1}{2} (L^+ S^- + L^- S^+) + L_z S_z \right] \quad (1)$$

was included in the Hamiltonian after self-consistency was reached. The relations between the spin-orbit parameter and the atomic spin-orbit splittings are

$$\begin{aligned} E(p_{3/2}) - E(p_{1/2}) &= \frac{3}{2} \lambda_p, \\ E(d_{5/2}) - E(d_{3/2}) &= \frac{5}{2} \lambda_d. \end{aligned} \quad (2)$$

We chose $\lambda_p = 0.67$ eV for the I $5p$ states close to the observed splittings in atomic spectra of I,³¹ and of exciton spectra of other ionic insulators, such as KI.³² Based on the analysis of our He II spectra of the Cd $4d$ states (Sec. V E) we chose $\lambda_d = 0.26$ eV.

In the ASW method the crystal is subdivided into Wigner-Seitz spheres which surround each atom. Within each sphere the potential is taken spherically symmetric. This so-called muffin-tin approximation has proven to give quite reliable results for close-packed structures. However, layered compounds have structures which are far from close packed. A better approximation of the true crystal potential of these structures may be obtained by filling unoccupied states by Wigner-Seitz spheres which contain no nucleus.

In our calculation we have filled the empty octahedral sites in the van der Waals gap with such empty spheres, at the coordinates $(0,0,\frac{1}{2}c)$ for $2H\text{-CdI}_2$ and $(0,0,\frac{1}{4}c)$ and $(\frac{1}{2}a\sqrt{3},0,\frac{3}{4}c)$ for $4H\text{-CdI}_2$. The set of basis functions which was used consisted of Cd $5s$, $5p$, and $4d$ functions: I $5s$ or $6s$, $5p$, and $5d$ functions; and $1s$, $2p$, and $3d$ functions in the empty spheres. I $5s$ basis functions were used in the calculation of the valence states, while I $6s$ basis functions were used in the calculation of the unoccupied states. In the ASW program it is not possible to include I $5s$ and I $6s$ states simultaneously. The inclusion of I $6s$ states was of little influence on the I $5p$ -derived valence states. The shifts were less than 0.1 eV, except for the lowest band, which was shifted downwards by 0.2–0.3 eV. This I $5p_z$ –I $6s$ hybridization causes a polarization on the I atoms towards the Cd layer, which results in a non-spherical potential. In the self-consistency procedure this effect is not taken into account. Therefore we expect that nonsphericity corrections would reduce the shift of the I p_z state to 0.1–0.2 eV. The unoccupied states were very sensitive to the inclusion of I $6s$ states. Shifts up to 1 eV were observed for states in the Cd $5s$ -derived band. An occupation of 0.08 I $6s$ states/atom was found. In the calculation of the three-center integrals, $4f$ wave functions of Cd, I, and the empty spheres were included. This can be regarded as treating $4f$ functions as a perturbation.

By using the ASW method, *ab initio* band-structure calculations can be performed. The only input parameters are the atomic positions, the crystal structure, lattice parameters, and Wigner-Seitz radii. In Table I the lattice parameter and Wigner-Seitz spheres which were used in the calculations are tabulated. The length of the a axis is somewhat smaller than the experimental value, in order to

TABLE I. Input parameters for the ASW calculation.

Lattice constants	$2H\text{-CdI}_2$	$a = 4.180 \text{ \AA}$
		$c = 6.736 \text{ \AA}$
		$z = 0.25$
		$c/a = 1.611$
	$4H\text{-CdI}_2$	$a = 4.180 \text{ \AA}$
		$c = 13.472 \text{ \AA}$
		$z = 0.125$
		$c/a = 3.223$
Wigner-Seitz sphere radii	Cd	1.430 \AA
	Ze	1.634 \AA
	I	2.043 \AA

minimize the total energy. The c/a ratio is equal to the experimental value.

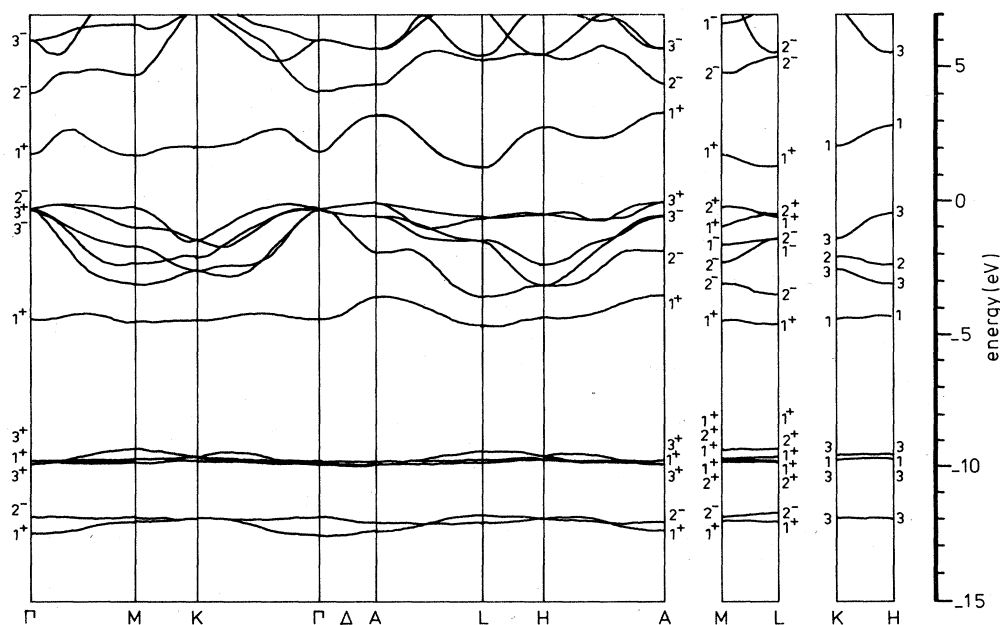
It was found that omission of the empty spheres has its largest effect on the lowest valence band. Upward shifts from 0.3 to 0.6 eV were observed. All other shifts in the valence band are less than 0.3 eV. The conduction bands are more sensitive to this change of the potential: shifts up to 0.9 eV are observed. Similar effects were observed to result from a change in the ratio of the Wigner-Seitz sphere radii. The sensitivity of the lowest valence band to the details of the potential can be understood easily from the fact that it consists of I p_z -bonding states, which have an appreciable density in the van der Waals gap. The potential in the gap region may depend heavily on the inclusion of empty spheres, and on the ratio of the Wigner-Seitz spheres. A similar explanation can be given for the large effects on the states in the conduction band, which are rather delocalized.

B. Band-structure calculation of $2H\text{-CdI}_2$

The calculated energy bands along symmetry lines in the Brillouin zone [Fig. 2(b)] are plotted in Fig. 4 (without spin-orbit interaction) and in Fig. 5 (including spin-orbit interaction). The symmetry notation of Miller and Love³³ was used. The combinations of atomic (s, p, d) functions which transform to each of the irreducible representation of the group of the wave vector have been tabulated by Murray, Bromley, and Yoffe.³⁴ The same notation has been adopted by Mattheiss.³⁵ As the crystal has inversion symmetry, even when spin-orbit interaction is included, each band is at least twofold degenerate due to time reversal symmetry (Kramers degeneracy).

The total density of states (DOS) is shown in Fig. 6. The decomposition of the DOS according to atom and angular momentum is given in Fig. 7. In these figures the energy zero in eV has been placed at the top of the valence band.

The band at about -12 eV is predominantly of I $5s$ character. It has a width of 0.8 eV. The Cd $4d$ band is found at 9.9 eV below the top of the valence band. Its total width of 0.8 eV is not only due to spin-orbit coupling (0.5 eV, Sec. IV A), but also to interaction with I states (see Fig. 7).

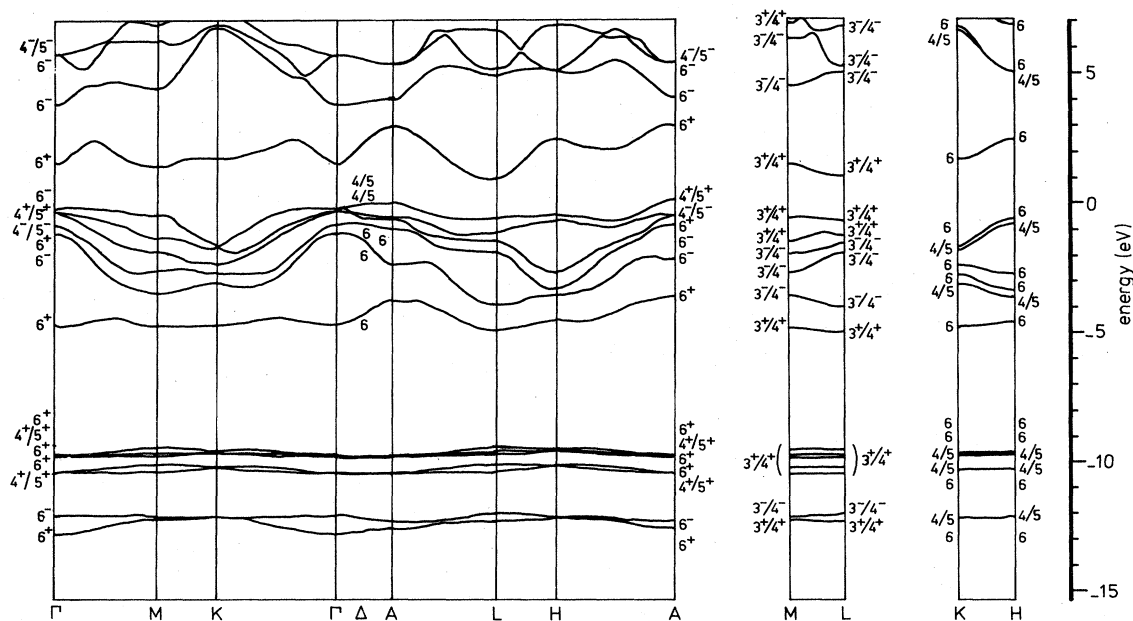
FIG. 4. Band structure of $2H\text{-CdI}_2$, without spin-orbit interaction.

The valence band has mainly I $5p$ character. Its calculated width is 4.9 eV.

The band from 1.2 to 3.8 eV has mainly Cd $5s$ character. Bands with Cd $5p$ character, strongly hybridized with I $5d$ states, are found above 4.8 eV.

The calculated direct gap between the valence band and the conduction band is 1.6 eV ($L_3^+/L_4^+ \rightarrow L_3^+/L_4^+$). The calculated indirect gap is 1.0 eV ($A_4^+/L_5^+ \rightarrow L_3^+/L_4^+$).

The observed optical-absorption edge for direct transitions is 3.8 eV,¹⁹ the indirect optical gap (at room temperature) is 3.2 eV.¹⁹ Pure CdI_2 crystals are transparent. The calculated direct and indirect gaps are 60% too small compared to the experimental value. An underestimation of the gap is frequently encountered in self-consistently band-structure calculations of semiconductors and insulators, which use the local-spin-density (LSD) approxima-

FIG. 5. Band structure of $2H\text{-CdI}_2$, including spin-orbit interaction.

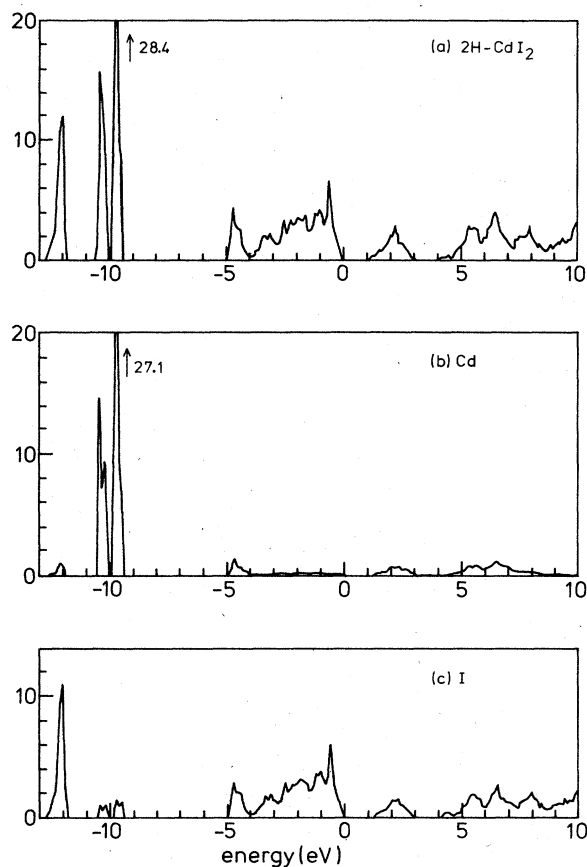


FIG. 6. (a) Total density of states of $2H\text{-CdI}_2$. (b) Cd site projected density of states; (c) I site projected density of states. Units: states/eV unit cell.

tion (see, e.g., Ref. 36). Perdew and Zunger³⁷ have attributed this discrepancy to the fact that in the LSD method the self-Coulomb interaction is not exactly canceled by the self-exchange interaction, and have intro-

duced a method to calculate the self-interaction correction (SIC). In a LSD calculation the energy of an electron in a conduction band is calculated using the ground-state potential, which is based on the charge density in the ground state. From this it follows that only for states in the valence band a SIC is needed. Because the SIC is always negative, it leads to enlarged band gaps. Until now, this method has been used successfully in atoms and in wide-gap insulators, but not in semiconductors with more delocalized states. In CdI_2 a rigid shift of 2.2 eV of the conduction band relative to the valence band yields a good agreement between the experimental and theoretical direct and indirect gaps.

In band-structure calculations of $2H\text{-CdI}_2$, reported by McCanny *et al.*,¹⁴ Bordas *et al.*,¹⁶ and Robertson,¹⁷ a semiempirical tight-binding method was used. Bandwidths and the band gap were adjusted to the results of optical and photoemission experiments. The basis set was limited in all cases to I $5s$, I $5p$, Cd $5s$, Cd $5p$, and in one case it also included Cd $4d$ (McCanny *et al.*). Spin-orbit interaction was not taken into account. Although the general shape of the valence bands of these calculations is basically the same as that of our calculation, differences up to 1 eV of the position of these bands are observed. Probably due to the omission of I $5d$ states from the basis set of the tight-binding calculations, the general shape and energy position of the states in the conduction bands are entirely different from our calculation. From Fig. 7 it can be seen that the Cd $5s$ and $5p$ bands are strongly hybridized with I $5d$ states.

C. Band structure of $4H\text{-CdI}_2$

The band structure of $4H\text{-CdI}_2$ was calculated using the same Wigner-Seitz radii as in the calculation of $2H\text{-CdI}_2$. The band structure is shown in Fig. 8. Spin-orbit interaction was not included in the calculation, so Fig. 8 should be compared to Fig. 4. For comparison with experiment we will show in Sec. V the calculated bands along lines of

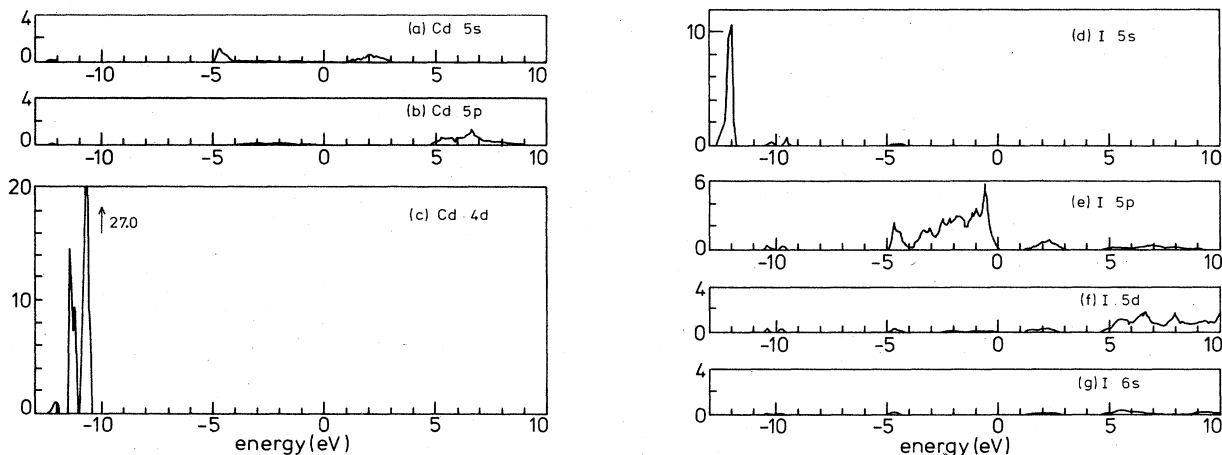
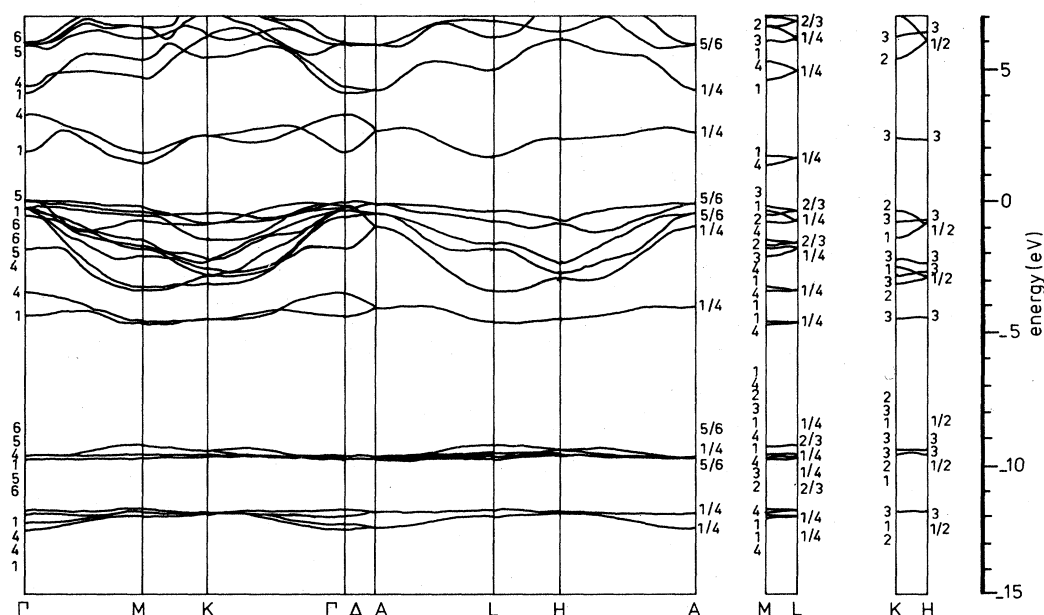


FIG. 7. Atom and angular momentum decomposed density of states of $2H\text{-CdI}_2$. Units: states/eV unit cell.

FIG. 8. Band structure of $4H$ - CdI_2 , without spin-orbit interaction.

constant $k_{||}$, including spin-orbit interaction.

The $2H$ and $4H$ polytypes are different with respect to the stacking of the I-Cd-I layers. The crystal structure within these layers remains the same. As the bonding between the layers is weak, no large differences in the band structure of both polytypes are expected. An effect of the doubling of the c axis of $4H$ - CdI_2 compared to $2H$ - CdI_2 is that the c^* reciprocal-lattice vector is reduced to one-half of its original length. In a reduced zone scheme bands along a direction parallel to the k_z axis are folded back around the k point ($k_{||}, c^*(2H)/4$), where

$$c^*(2H) = \frac{2\pi}{c(2H)}.$$

This leads to a doubling of the number of bands, consistent with the double number of atoms per unit cell. It

also leads to a (at least) twofold degeneracy per spin direction at points in the upperplane of the Brillouin zone (ALH plane). The band structure of the $4H$ - CdI_2 at points in the ΓMK plane must be compared to a superposition of the band structure of $2H$ - CdI_2 in the ΓMK and ALH planes. The interesting point is to what extent interactions between the layers cause deviations from such a simple superposition. In Table II we have made such a comparison for the valence bands at Γ , M , and K . From Table II it follows that such a superposition gives a very good description of the band structure at Γ . All differences are smaller than a few hundreds of an eV. From the symmetry labels it can be seen that states which are folded back from A (Γ_4 and Γ_5) do not interact with states which originate from the $2H$ - CdI_2 Γ point (Γ_1 and Γ_6). The second column of Table II shows that such an in-

TABLE II. Comparison of $2H$ - CdI_2 and $4H$ - CdI_2 band structure at Γ , M , and K . Spin-orbit interaction is not included. Energies with respect to the top of the valence band, in eV. $\Gamma(A)_3^+$, $\Gamma(A)_3^-$, and $K(H)_3$ are twofold degenerate states for $2H$ - CdI_2 . Γ_5 , Γ_6 , and K_3 are twofold degenerate states for $4H$ - CdI_2 .

Γ				M				K			
$2H$		$4H$		$2H$		$4H$		$2H$		$4H$	
Γ_1^+	-4.36	Γ_1	-4.34	L_1^+	-4.65	M_4	-4.63	K_1	-4.44	K_3	-4.47
A_1^+	-3.45	Γ_4	-3.45	M_1^+	-4.50	M_1	-4.58	H_1	-4.34		
A_2^-	-1.82	Γ_4	-1.80	L_2^-	-3.55	M_1	-3.40	H_3	-3.13	K_2	-3.12
A_3^-	-0.53	Γ_5	-0.54	M_2^-	-3.07	M_4	-3.26			K_3	-2.81
Γ_3^-	-0.30	Γ_6	-0.31	M_2^-	-2.31	M_1	-2.09	K_3	-2.54	K_1	-2.54
Γ_3^+	-0.25	Γ_6	-0.24	M_1^-	-1.69	M_3	-1.69	H_2	-2.36	K_3	-2.23
Γ_2^-	-0.14	Γ_1	-0.14	L_1^-	-1.48	M_3	-1.49	K_2	-2.04		
A_3^+	0	Γ_5	0	L_2^-	-1.37	M_4	-1.81	K_3	-1.41	K_1	-1.41
				M_1^+	-0.95	M_4	-0.78			K_3	-0.83
				L_1^+	-0.61	M_1	-0.39	H_3	-0.39	K_2	-0.40
				L_2^+	-0.52	M_2	-0.52				
				M_2	-0.21	M_3	-0.20				

interaction does occur for states at the M point, provided that they contain I p_z character. These M_1 and M_4 states with M_1^+ , M_2^- , L_1^+ , or L_2^- symmetry in $2H$ -CdI₂ have interaction energies up to 0.44 eV (L_2^- at -1.37 eV versus M_4 at -1.81 eV). The M_2 or M_3 states, with M_2^+ , M_1^- , L_2^+ , or L_1^- symmetry in $2H$ -CdI₂ contain no I P_z character. Their interaction energies are less than a few hundreds of an eV. For points P on the line KH in the Brillouin zone, drastic effects of the different symmetry of $2H$ - and $4H$ -CdI₂ are observed. Bands with P_1 symmetry (from K_1 to H_1 and K_2 and H_2) in $2H$ -CdI₂, form a twofold degenerate band with P_3 symmetry in $4H$ -CdI₂. Bands with P_2 and P_3 symmetry (from K_3 to H_3) which are time-reversal degenerate in $2H$ -CdI₂, split up into bands with P_1 , P_2 , and P_3 symmetry in $4H$ -CdI₂. The third column in Table II shows that in spite of the large changes of the shapes and degeneracies of the bands, the widths and centers of mass of the bands are hardly different.

It is concluded that effects of polytypism on the band structure are negligible at the center of the zone (and in general along ΓA). At the zone edges, effects up to 0.5 eV have been calculated. A similar conclusion followed from tight-binding calculations of the band structures of three polytypes of GaSe by Nagel *et al.*³⁸

Another aspect of the difference of the $2H$ and $4H$ crystal structures is the inequivalence of the two pairs of I atoms in the unit cell of the $4H$ polytype. I atoms at $2a$ sites have a fcc-like coordination of nearest I atoms, while the coordination around $2b$ sites is hcp-like. This results in slightly different charges of the atoms: -0.323 and -0.327 , respectively. The Cd charge is $+1.227$ and the charge within the empty sphere is -0.577 . It has to be kept in mind that these charges depend on the choice of the Wigner-Seitz radii. For the $2H$ polytype the calculated charges for I, Cd, and the empty sphere are -0.323 , $+1.235$, and -0.588 , respectively.

V. ANGLE-RESOLVED PHOTOEMISSION FROM CdI₂

A. Theory of ARUPS

Reviews of the methods and results of determining band structures from ARUPS spectra and of the theory of the photoemission process have been given by Feuerbacher, Fitton, and Willis,³⁹ Petroff,⁴⁰ Smith,⁴¹ and Himpsel.⁴² Here we limit ourselves to a short outline of the band-mapping technique and a discussion of those aspects of the theory and photoemission that are relevant to this study.

The binding energy E_b of an electron that has absorbed a photon with energy $\hbar\omega$ can be calculated from its kinetic energy outside the solid using the law of energy conservation:

$$E_b = \hbar\omega - E_{\text{kin}} - \Phi, \quad (3)$$

where Φ is the work function. The binding energy is defined as the ionization potential with respect to the Fermi energy. The component of the wave vector k_{\parallel} parallel to the surface is conserved upon the transmission through

the surface. Its magnitude can be calculated using the relation

$$k_{\parallel} = \frac{1}{\hbar} (2mE_{\text{kin}})^{1/2} \sin\theta \quad (4)$$

from E_{kin} and θ , the angle which the outgoing electron makes with the normal to the surface of the solid. As the solid-vacuum system has no symmetry for translations normal to the surface, k_{\perp} is not conserved at the surface.

Due to the very short electron mean free path, which is about 10 Å for electrons at 20 eV above the Fermi level, the relevant excitation processes take place in the first few atomic layers of the solid. Therefore, the three steps into which the photoemission process is often subdivided, the excitation process, the transport of the electron to the surface, and the transmission of the electron through the surface, are coherent processes which have to be described in a single-step theory.⁴³⁻⁴⁷ From these theories it follows that depending on the electron mean free path the photoemission process can be described either using a direct transition model, in which k -conserving transitions are dominant, or using an indirect model, in which k_{\perp} is completely undetermined. The direct transition model has been used successfully in the interpretation of ARUPS spectra of the noble metals and III-V semiconductors. The indirect transition model has been used in the interpretation of ARUPS spectra of the lead chalcogenides⁴⁸ and the layered compound NbSe₂.⁴⁹ In that limit the spectra are proportional to the one-dimensional density of states (ODDOS) along the perpendicular direction, $(\partial E / \partial k_{\perp})^{-1}$, modified by matrix-element effects. The two models can be distinguished by a study of the peak positions as a function of the photon energy. For normal emission, only in the direct transition model is an energy dependence expected.

From an analysis of ARUPS spectra with a single-step model in principle much can be learned about the effects of inelastic scattering on the widths and line shapes of the peaks, and about surface effects such as emission from surface states and surface resonances and so-called band-gap emission from evanescent waves.⁵⁰ However, in practice it is often not clear which structure in the calculated spectra is due to bulk photoemission or to surface effects.

For layered compounds, surface effects are expected to be less important than, e.g., for the III-V semiconductors or the noble metals, as the interactions between the layers are small. Therefore single-step calculations of the ARUPS spectra of these compounds should give more easily interpretable information about matrix element, lifetime, and scattering effects on the bulk photoemission spectrum. Until now only Liebsch⁵¹ has performed such a study, in which he successfully calculated the azimuthal intensity distribution of electrons from the d band in TaS₂.

Because of the elevated temperature at which the ARUPS spectra were measured, it is relevant to discuss the effects of temperature on the spectra. The theory of the effect of electron-phonon interactions on the initial and final states, and on the photoemission process, has been treated by Shevchik.⁵² It is found experimentally and theoretically that the effect of temperature on the ini-

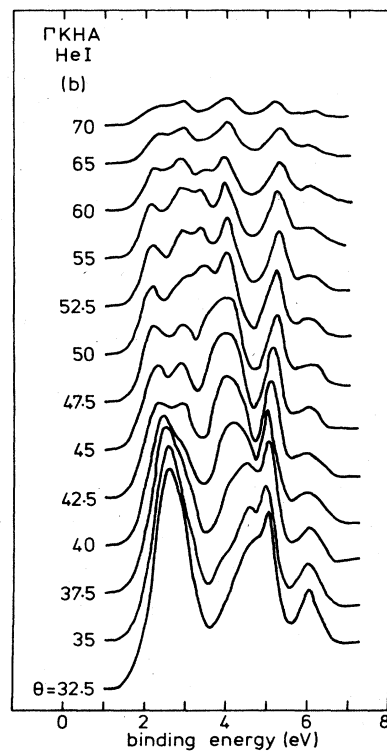
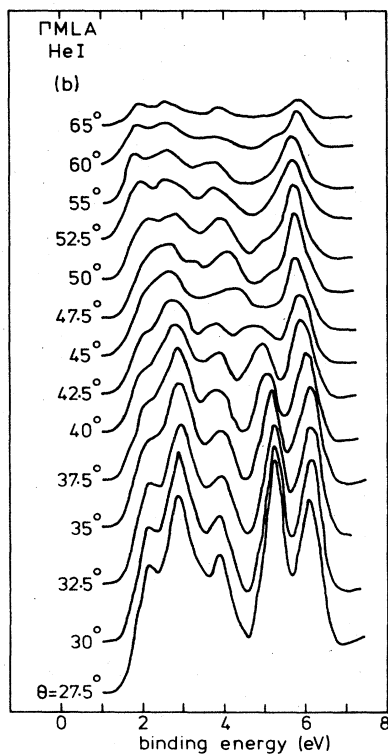
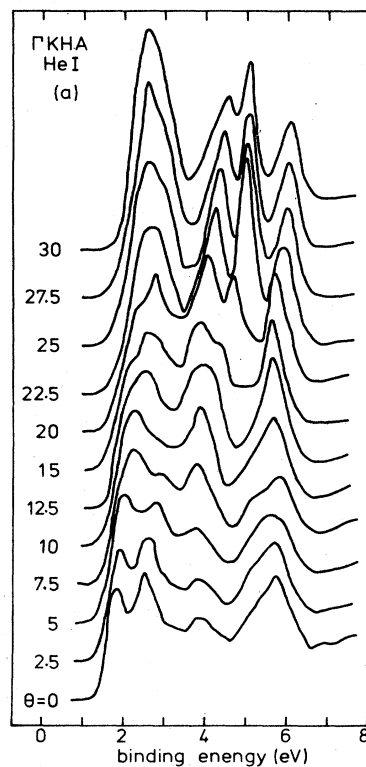
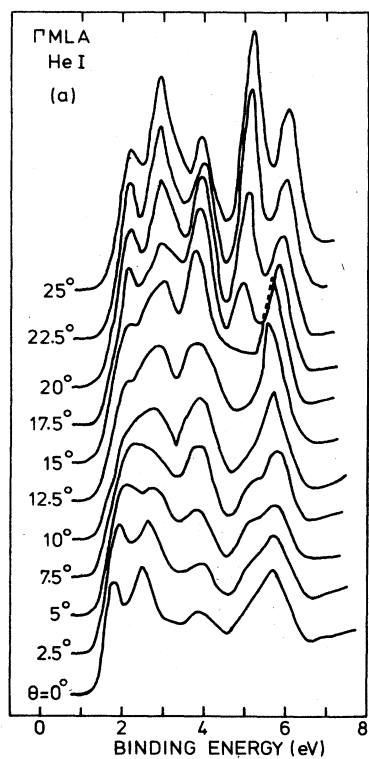


FIG. 9. ARUPS spectra of 4H-CdI₂, at $\alpha=15^\circ$, for electrons emitted to the Γ MLA plane, as a function of the emission angle θ .

FIG. 10. ARUPS spectra of 4H-CdI₂, at $\alpha=15^\circ$, for electrons emitted in the Γ KHA plane, as a function of the emission angle θ .

tial states is a shift and a lifetime broadening caused by electron-phonon interactions in the valence band. The observed shifts are of the order of 0.5 meV/K. Phonon-assisted transitions cause a weakening of the \mathbf{k} -selection rules, eventually leading to an angle-integrated spectrum at temperatures far above the Debye temperature.

B. Experimental results—valence-band spectra

Figures 9 and 10 show the ARUPS spectra, which were measured using HeI radiation, for the ΓM and ΓK direction, respectively. The angle of photon incidence was $\alpha=15^\circ$. Only the valence-band region is shown. The binding energy is relative to the Fermi level, which lies in the gap and is probably pinned by impurity and defect states.

In Figs. 11 and 12 the measured peak positions in the HeI valence-band spectra are plotted versus k_{\parallel} , for the $\Gamma M L A$ and $\Gamma K H A$ emission planes, respectively. These plots were constructed using Eqs. (3) and (4). Open circles denote weak shoulders. The threshold energy (energy distance from the vacuum level to the top of the valence band) was determined to be 6.8 ± 0.3 eV. From Figs. 11 and 12 it can be seen that the peak positions in the second Brillouin zone are the same, within the experimental error, as those at equivalent \mathbf{k} points in the first zone. In some cases peaks that are seen in one of the zones, are not present at the equivalent \mathbf{k} point in the other zone. We ascribe this to matrix-element effects. ARUPS spectra were also measured at constant polar angle $\theta=30^\circ$ and variable azimuth angle φ . The peak positions as a function of φ are shown in Fig. 13. The measurements correspond approximately to measurements in the $MLHK$ plane, at the edge of the Brillouin zone. Therefore, the measured dispersion of the peak positions can be compared to the dispersion along KM in Fig. 12. These two measurements agree very well.

C. Comparison with calculated band structures

In Fig. 14 we have plotted the calculated band structure of $2H\text{-CdI}_2$ as a function of k_z , at constant k_{\parallel} . The experimental peak positions are given as circles in these fig-

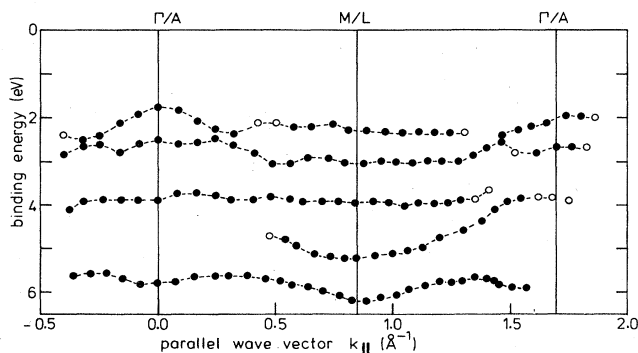


FIG. 11. Peak positions as a function of k_{\parallel} for $4H\text{-CdI}_2$, measured with HeI radiation and $\alpha=15^\circ$, for emission in the $\Gamma M L A$ plane.

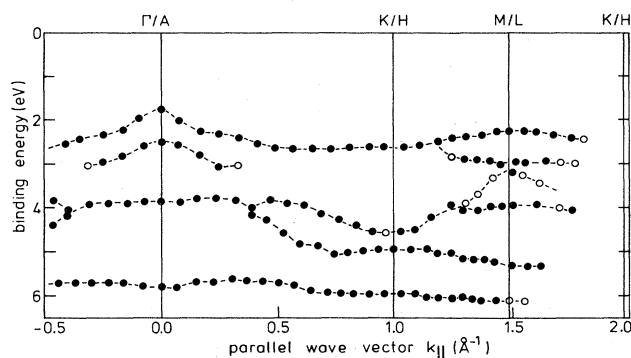


FIG. 12. Peak positions as a function of k_{\parallel} for $4H\text{-CdI}_2$, measured with HeI radiation and $\alpha=15^\circ$, for emission in the $\Gamma K H A$ plane.

ures. As for these peak positions k_z is not known, all circles are plotted at $k_z = \frac{1}{2}\pi/c$. In the $\Gamma M L A$ plane the \mathbf{k} points (k_{\parallel}, k_z) and $(k_{\parallel}, -k_z)$ are inequivalent. The dashed line is the band structure in the k_z interval $(0, -\pi/c)$. The energy zero in these plots is the calculated top of the valence band at A , whereas the experimental peak positions were shifted in such a way that the one-but-lowest experimental peak at $M L$ coincides with the center of mass of the calculated band at -3.75 eV. The “calibration point” has been chosen because of the insensitivity of this band to changes of the potential and because of its small width (0.4 eV). In Figs. 9 and 10 the new energy zero now lies at -1.50 eV binding energy.

For a detailed comparison between theory and experiment, we will first look at the lowest band, which can be characterized as a bonding $I p_z$ band. Especially at the edge of the zone, such a comparison is easy because of the small dispersion of this band. It can be concluded that the experimental peak positions follow the dispersion of the center of mass of the calculated bands, from $\Gamma (A)$ to $M (L)$, from $\Gamma (A)$ to $K (H)$, and from $K (H)$ to $M (L)$ closely, but that the theoretical energy is 0.2–0.25 eV too low at all \mathbf{k} points. Such an effect is not surprising as this is the band which is the most sensitive to the treatment of

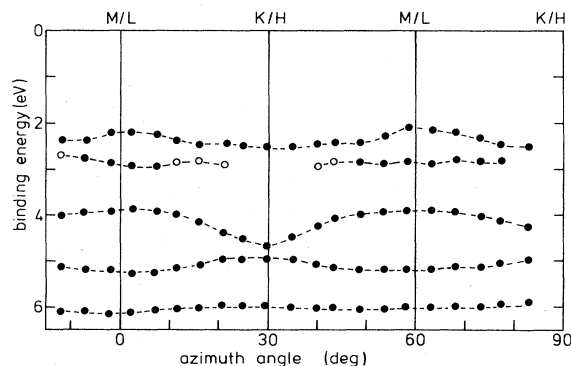


FIG. 13. Peak positions of HeI spectra of $4H\text{-CdI}_2$ at $\theta=30^\circ$ and $\alpha=15^\circ$, as a function of the azimuth angle φ . Effectively the band structure along the edge of the zone ($MLHK$ plane) is measured (see text).

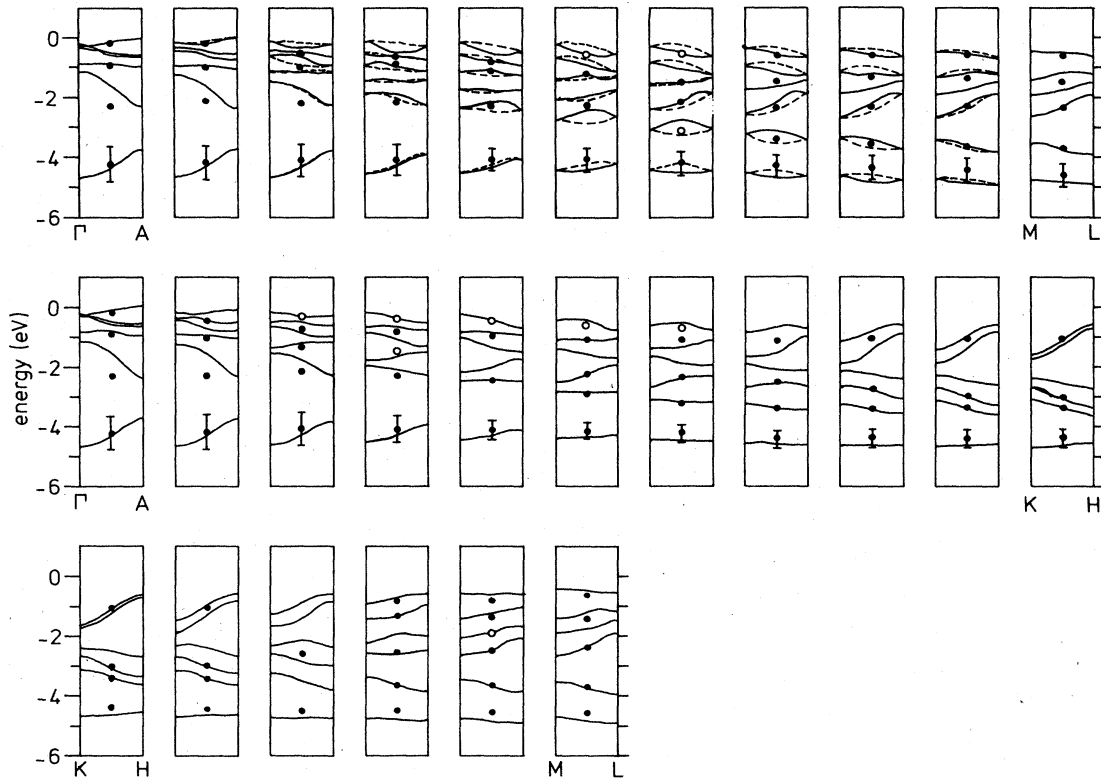


FIG. 14. Band structures of $2H\text{-CdI}_2$ (including spin-orbit interaction), as a function of k_z . The upper part of the figure gives the band structures at equidistant k_{\parallel} points along the ΓM direction. In each diagram k_z ranges from 0 to π/c (solid line) or from 0 to $-\pi/c$ (dashed line). The middle and lower part of the figure give the band structure for k_{\parallel} point along ΓK and KM , respectively, for which $E(\mathbf{k}_{\parallel}, k_z) = E(\mathbf{k}_{\parallel}, -k_z)$. Experimental peak positions (from Figs. 12 and 13) are indicated by solid circles. Open circles are weak shoulders.

the potential in the van der Waals gap (Sec. IV A). Error bars in Fig. 14 give the width at half height of the experimental peaks. These widths correlate with the calculated dispersion along the k_z direction. From the experimental line width k_{\parallel} directions where the calculated dispersion is very small, e.g., along ΓK near K , it can be concluded that the total broadening is 0.65 ± 0.05 eV full width at half maximum. The broader peak in the normal emission spectrum can be explained in an indirect transition model, leading to a ODDOS-shaped peak.

The one but lowest band is also observed very well in the spectra. Its peak positions agree well with the calculated energies. Near Γ this band is broader than the calculated total broadening. The peak in the normal emission spectrum at -2.3 eV is a very good candidate for an experimental determination of the transition model using a tunable photon-energy source. The observed position of the peak can be explained with an indirect model. However, if the peak were due to direct positions, an easily measurable dependence of the peak position on the excitation energy is expected [see Fig. 15(a)].

Contrary to the two lower bands, Fig. 14 shows that the four higher bands have a dispersion in the k_z direction which is comparable, and sometimes larger, than the distance between these bands. In that case an assignment of

each experimental peak to a critical point, or a whole band if the total broadening is larger than the bandwidth, is not always possible. We show therefore in Fig. 15 the complete spectra (not only peak positions) that are calculated from the experimental spectra using (3) and (4), together with the calculated band structures of $2H\text{-}$ and $4H\text{-CdI}_2$. For this comparison we have chosen six k_{\parallel} directions, for which the band structures have been plotted as a function of k_z . Figure 16 gives their positions in the Brillouin zone. Spectra at two equivalent ML points [(1) and (2) in Fig. 15(c)] are compared with each other.

(a) In the ΓA spectrum the double peak between 0 and -1.3 eV corresponds to the four upper bands and to the upper part of the one-but-lowest band. From a comparison of Fig. 8 with the lower part of Fig. 15(a) it can be seen that the distance between the two peaks is a measure of spin-orbit splitting. The good agreement between theory and experiment justifies our choice of the spin-orbit parameters λ_p . A simple ODDOS theory cannot explain the dip in the spectrum at -0.5 eV. It is probably due to different transition probabilities from each of the four upper bands. The dependence of these transition probabilities on the angle of photon incidence are described in Sec. VD. Because of the relatively small difference between the $2H$ and $4H$ band structures, it is

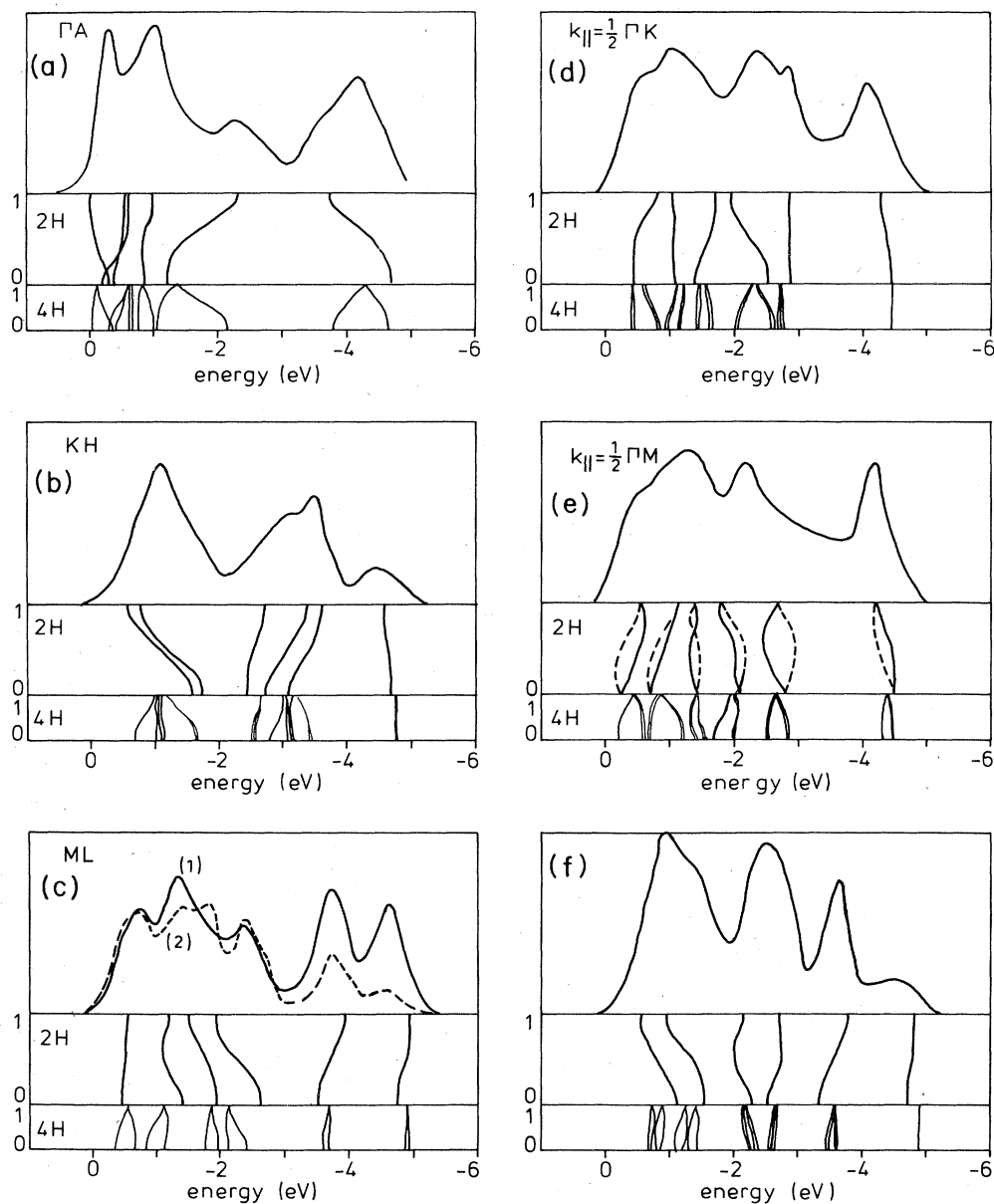


FIG. 15. (a)–(f) Experimental spectra and band structures for 2H- and 4H-CdI₂ (including spin-orbit interaction), at six k_{\parallel} directions (see Fig. 16).

not possible to deduce from the spectrum which band structure is the most appropriate.

(b) The KH spectrum reflects the three parts into which the band structure from K to H is subdivided. The spectrum confirms the calculated energy position of the five highest bands. If a ODDOS is measured the upper peak at -1.0 eV would have been expected to consist of two parts, at least in 2H-CdI₂. The 4H-CdI₂ calculation gives a better explanation of the observation of a single peak.

(c) The spectra at the two equivalent ML points differ mainly by the appearance of a peak at -1.9 eV in spectrum $c2$. The low relative intensity at the low-energy side of spectrum $c2$ is due to the fact that this spectrum is

composed of experimental spectra at $\theta=50^\circ$ at the top of the valence band up to $\theta=65^\circ$ at the bottom, a range in which the photoelectron intensity decreases rapidly. The gap in the band structure from about -2.5 to -3.5 eV is clearly seen in both spectra. The 4H calculation gives a good description of the structure in spectrum 1 above -2.5 eV if the four upper bands are shifted about 0.3 eV to lower energy. In particular this could explain the dip in the spectrum between the maxima at -1.3 and -2.3 eV. The appearance of the extra peak in spectrum 2 would then not be explicable in terms of the 4H band structure. This could be an effect of the different effective mean free path of the photoelectrons, with $\lambda=10$ Å,

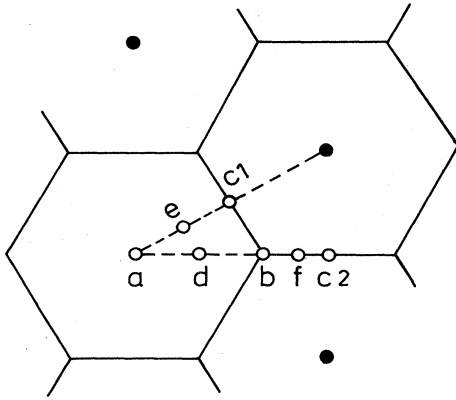


FIG. 16. $k_{||}$ points for which in Fig. 15 a comparison is made between theory and experiment.

$\lambda_{\text{eff}} \approx 9$ Å in spectrum 1, and $\lambda_{\text{eff}} \approx 6$ Å in spectrum 2. In the case of spectrum 2, λ_{eff} is much smaller than the unit-cell thickness ($c = 13.7$ Å) of $4H\text{-CdI}_2$. The photoelectrons effectively probe only the first layer, and this will result in a different spectrum. However, an explanation of the extra peak is also possible if only the second and fourth bands of $4H\text{-CdI}_2$ are shifted downward, assuming that matrix-element effects prohibit photoemission from the third band. The appearance of the extra peak in spectrum 2 is then a matrix-element effect.

(d) For $k_{||} = \frac{1}{2}\Gamma K$ the peaks at -0.6 , -1.1 , and -2.9 eV correspond to rather flat bands which are within 0.3 eV of the experimental peak position. The dip in the spectrum at -1.8 eV is best explained by the $4H$ calculation.

(e) In the spectrum at $k_{||} = \frac{1}{2}\Gamma M$ we assign the peak at -2.2 eV to the fourth band in $2H\text{-CdI}_2$ (counted from the top of the valence band). Its calculated position seems to be 0.2–0.4 too high, but from Fig. 14 it can be seen that the experimental angular resolution combined with the high dispersion of the fourth and the fifth band might cause such deviations between theory and experiment. Bands 1–3 are seen as a broad peak with a weak shoulder at -0.5 eV. Probably due to matrix-element effects, band 5 is seen very weakly in the spectrum, at about the calculated energy position. Its intensity rises strongly on going to $k_{||} = \Gamma M$.

(f) The spectrum for $k_{||}$ between ΓK and ΓM , at the edge of the zone, consists of four peaks, which can be assigned easily to the calculated bands. The differences be-

tween the calculated centers of mass of the bands and the peak positions are less than 0.2 eV, except for band 6. In general, the bands of $4H\text{-CdI}_2$ are narrower than those of the $2H$ structure, but the spectrum can be understood from both calculations.

From this analysis of the ARUPS spectra we conclude that the peak positions can be described very well in terms of the $4H\text{-CdI}_2$ band structure. In some cases, (e.g., the lowest valence band) a significant difference between peak positions and calculated band energies has been observed. These differences are smaller than 0.3 eV. The observed peak widths are highly correlated to the calculated bandwidths, pointing at indirect transitions. The resulting spectra resemble a one-dimensional density of states, broadened by lifetime and thermal effects. However, conclusive evidence for an indirect transition model can only be obtained from spectra as a function of the photon energy. Compared to the spectra of McCanny *et al.*,¹⁴ our spectra have a much better energy resolution, which made a more detailed analysis of the spectra possible. Differences with their spectra may be due to matrix-element effects, as they used a photon incidence angle $\alpha = 60^\circ$, while our spectra were taken at $\alpha = 15^\circ$.

D. Peak intensities and wave-function symmetry

The variation of the spectra with the angle of photon incidence α can give information about the wave-function character of the initial state, using dipole selection rules and the fact that the final state transforms according to the totally symmetric representation (Hermanson⁵³). For crystals with the $2H\text{-CdI}_2$ structure such an analysis can be performed for emission in the mirror plane $y=0$ in Fig. 1(a), which corresponds to emission in the $\Gamma ML A$ plane in reciprocal space. Dipole selection rules have been tabulated by Murray *et al.*³⁴ The initial-state symmetries are tabulated in Table III for single- and double-group representations.

In the mirror plane all states form twofold degenerate pairs which have the double-group representation F_3 and F_4 . No selection rules can be applied in this case. If spin-orbit interaction is relatively small, single-group selection rules make a discrimination between states with F_1 and F_2 symmetry possible. In our experimental setup with unpolarized radiation (Fig. 3) the x component of the polarization is proportional to $\cos\alpha$, and the z component is proportional to $\sin\alpha$, while the y component does not depend on α . From Table III it can be seen that if the initial state has F_2 symmetry, the peak intensity

TABLE III. Polarization dependence of photoelectron initial states for $2H\text{-CdI}_2$, space group D_{3d}^{34} in single- and double-group representations. Representations that are separated by a slash are time-reversal degenerate.

Polarization	Normal emission		Initial state	
	Single	Double	Single	Mirror plane emission Double
x	Δ_3	$\Delta_6 + \Delta_4/\Delta_5$	F_1	F_3/F_4
y	Δ_3	$\Delta_6 + \Delta_4/\Delta_5$	F_2	F_3/F_4
z	Δ_1	Δ_6	F_1	F_3/F_4

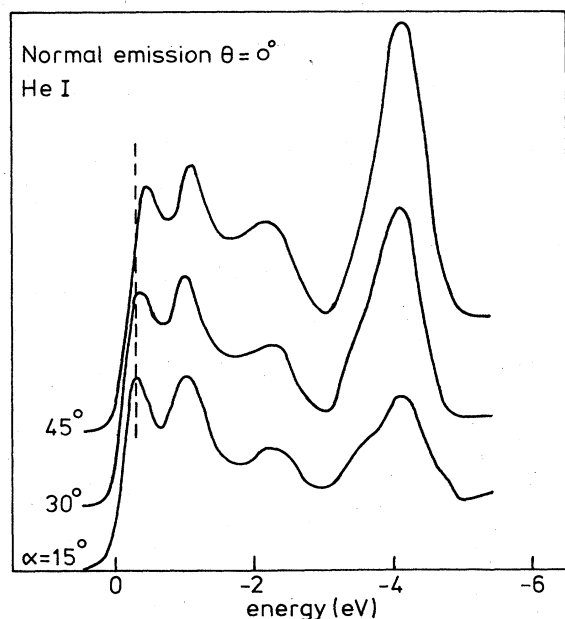


FIG. 17. He I normal emission spectra of 4H-CdI₂ as a function of the photon angle of incidence.

does not depend on α . If the initial state has F_1 symmetry, the peak intensity does depend on α and the intensity variation gives information about the amount of p_x and p_z character in the initial state.

We have performed such an analysis for states on the line Δ . In Fig. 17 spectra of CdI₂ at normal emission are shown as a function of the angle of photon incidence α . Although 4H-CdI₂ was used, for which the selection rules are much less restrictive, we will apply the rules for 2H-CdI₂, the band structure of which along Δ differs very little from that of the 4H polytype. The dispersiveness bands from Γ_1^+ to A_1^+ and from Γ_2^- to A_2^- in Fig. 4 have Δ_1 symmetry, being p_z bonding and antibonding states. The other bands, which are formed by p_x - and p_y -derived states, have Δ_3 symmetry. When spin-orbit interaction is included, Δ_3 splits up into $\Delta_4/\Delta_5 + \Delta_6$, and Δ_1 becomes Δ_6 (Fig. 5). As expected from the foregoing discussion, the two lower peaks at -2.3 and -4.2 eV become therefore more intense relative to the double peak between 0 and -1.2 eV, when α is increased, thereby confirming the $p_z(\Delta_6)$ character of the initial states. According to the band-structure calculation the lower of the double peak at -0.3 and -1.0 eV has more Δ_6 character than the upper peak. This is reflected in Fig. 17 as a relative intensity decrease and a negative shift of the upper peak as α is increased.

E. Cd 4d and I 5s lines

In Fig. 18 the He II spectrum of the Cd 4d line is compared with the DOS, calculated with a spin-orbit parameter $\lambda_d = 0.26$ eV (splitting 0.65 eV), and convoluted with a Gaussian with a full width at half maximum (FWHM) of

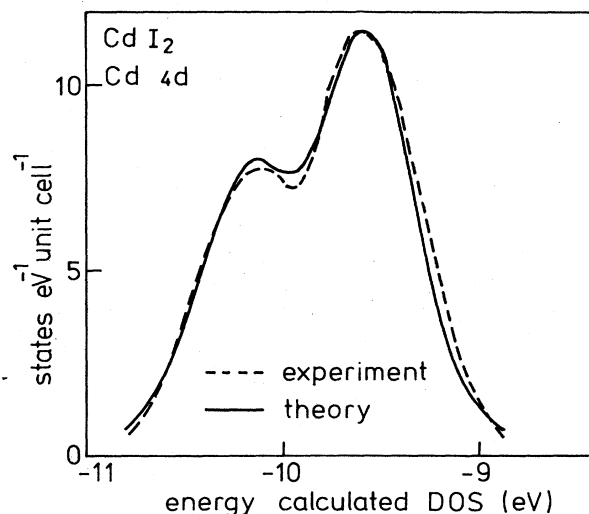


FIG. 18. Calculated density of states of the Cd-4d line of CdI₂ (solid line), convoluted by a Gaussian and a Lorentzian (see text). The dashed line gives the He II normal emission Cd 4d spectrum, shifted upwards by 0.1 eV in order to coincide with the calculated DOS.

0.40 eV and a Lorentzian with a FWHM of 0.2 eV. Within the experimental resolution this fit yields a good agreement of the peak separation (0.54 ± 0.04 eV), the peak intensity ratio ($d_{5/2}:d_{3/2} = 1.47 \pm 0.05$), and the total width at half height. The energy resolution (0.1 eV) is much better than in the x-ray photoelectron spectroscopy (XPS) spectra of Wertheim and Buchanan,⁵⁴ who did not resolve the two spin-orbit components. The contribution of thermal broadening to the total linewidth is approximately 0.3 eV, the difference between the total Gaussian broadening and the experimental resolution.

There has been some discussion about the Cd 4d spin-orbit splitting in the literature. Whereas the atomic splitting (Cd⁺) is 0.698 eV,³¹ for Cd metal the splitting is 0.95 ± 0.05 eV (data in Ref. 55), and the observed splitting for the cadmium chalcogenides is smaller, in the range 0.7–0.9 eV (data in Ref. 55). These differences have been attributed to a combined effect of spin-orbit splitting, crystal-field interaction, and hybridization with chalcogenide s levels in the case of the compounds,^{55–57} but no realistic quantitative study of this effect has been made until now. In the Appendix we will show that the apparent spin-orbit splitting of the 4d peak in Cd metal can be explained with a spin-orbit parameter $\lambda_d = 0.24$ eV (splitting 0.6 eV) in combination with a crystal-field splitting. This follows from relativistic ASW band-structure calculations of Cd metal. The spin-orbit parameter that is obtained in this way is in good agreement with the value for the atomic splitting and for CdI₂.

Like McCanny *et al.*,¹⁴ we did not observe the I 5s band in the He II spectra. It was also not observed in XPS spectra (Wertheim and Buchanan⁵⁴). McCanny *et al.* attribute these facts to the low cross section of these states for He II (uv) and Al K α (x-ray) photons. Indeed, from Scofield's tables⁵⁸ a cross-section ratio for 1487-eV photons (Al K α) of Cd 4d and I 5p state of 13.3 is found.

VI. CONCLUDING REMARKS

The comparison of the calculated band structure of CdI_2 and the ARUPS spectra yields a very good agreement if an indirect transition model is applied, but a final proof of the validity of the indirect transition model can be obtained only from accurate measurements at different photon energies. As most of the bands in the valence-band region have distances to other bands that are comparable to the bandwidth and the broadening by lifetime and temperature effects, an analysis which is only based on measured peak positions and calculated band structures along lines of high symmetry, as performed usually, would have been very difficult. Our analysis was based on a comparison of the complete spectra, not only peak positions, with the calculated band structure at the corresponding k_{\parallel} point as a function of k_z .

For some bands, small but significant discrepancies are observed between their experimental and theoretical position. This is especially true for the lower valence band whose calculated position is 0.2–0.25 eV too low. Such a discrepancy can be attributed to the difficulty of the band-structure calculation in dealing with the potential in the van der Waals gap. Compared to previous band-structure calculations of CdI_2 , the present calculation shows a much better agreement between theory and experiment. An important, but not the only reason for this better agreement is the inclusion of spin-orbit interaction in our calculation.

Note added in proof. A recent comparison of observed and calculated ASW band structures of transition-metal dichalcogenides showed that a much better agreement is obtained if effective z values for the anion positions are used in the calculations.⁶⁰ This effect is probably related with the polarization of the anion. For CdI_2 the main effect of a decrease of the z parameter is an increase of the calculated band gap. Therefore we conclude that, apart from self-interaction effects, the large difference between

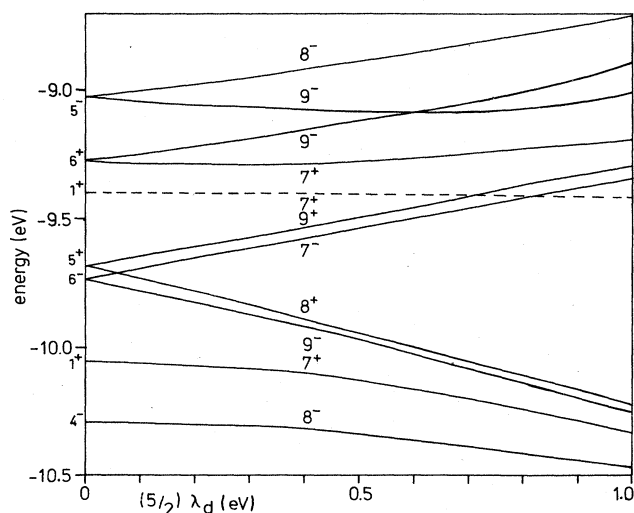


FIG. 19. Cd 4d states of Cd metal at point Γ in the Brillouin zone as a function of the spin-orbit parameter λ_d .

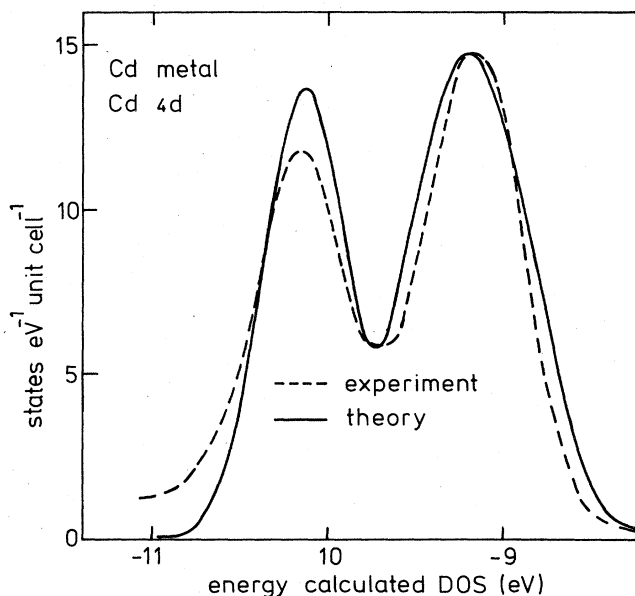


FIG. 20. Cd 4d DOS (solid line) broadened by a Gaussian (see text), compared with the HeII spectrum (from Ref. 57), dashed line. The experimental spectrum has been shifted upwards by 2.5 eV to coincide with the calculated DOS.

the experimental and calculated band gaps may also be due to the neglect of nonspherical components in the potentials.

ACKNOWLEDGMENTS

We are very grateful to A. Lenselink for providing the CdI_2 single crystals. One of us (R.C.) would like to thank the Stichting voor Fundamenteel Onderzoek van de Materie (FOM)—Bandenstructuur Berekeningen Instituut for the hospitality during his stay in Nijmegen. This investigation was supported in part by the Netherlands Foundation for Chemical Research (Stichting Scheikundig Onderzoek Nederlands, SON) and FOM with financial aid from the Netherlands Organization for the Advancement of Pure Research (Nederlandse Organisatie voor Zuiver-Wetenschappelijk onderzoek, ZWO).

APPENDIX

The combined effect of spin-orbit splitting and crystal-field splitting on the Cd 4d peak in the pure metal was investigated by self-consistent ASW band-structure calculations of the metal for different spin-orbit parameters λ_d . In Fig. 19 the eigenvalues of d states at the Γ point are plotted as a function of λ_d . The states have been labeled according to the convention of Miller and Love³³ for the double-group representations of the space group $P_{63}/mmc-D_{6h}^4$. Also, the single-group notations for $\lambda_d=0$ are shown. The dashed state has mainly Cd 5s character. The figure shows clearly that the crystal-field splitting is large, and that it considerably enhances the apparent spin-orbit splitting. A reasonable fit to the experimental spectrum was obtained by broadening the DOS

calculated with $\lambda_d = 0.24$ eV by a Gaussian with FWHM of 0.45 eV (Fig. 20). Further improvement of the fit is possible by using a Doniach-Sunjić line shape⁵⁹ (including asymmetric lifetime broadening due to many-body response of conduction electrons to the core hole). The experimental $d_{5/2}$ peak has been shifted from -11.7 to

-9.2 eV, in order to coincide with the theoretical peak. We attribute this difference to relaxation effects and the lack of a self-interaction correction (SIC), Sec. IV B, in the calculation. It is remarkable that for CdI_2 only a difference of 0.1 eV is observed between the calculated and experimental Cd $4d$ position (Fig. 18).

- ¹P. M. Williams, *Nuovo Cimento B* **38**, 216 (1977).
- ²I. T. McGovern, W. Eberhardt, E. W. Plummer, and J. E. Fischer, *Physica (Utrecht)* **99B**, 415 (1980).
- ³P. K. Larsen, S. Chiang, and N. V. Smith, *Phys. Rev. B* **15**, 3200 (1977).
- ⁴J. F. McGilp and A. W. Parke, *Phys. Status Solidi B* **94**, 685 (1979).
- ⁵D. R. Lloyd, C. M. Quinn, N. V. Richardson, and P. M. Williams, *Commun. Phys.* **1**, 11 (1976).
- ⁶I. T. McGovern, A. Parke, and R. M. Williams, *J. Phys. C* **9**, L511 (1976).
- ⁷P. K. Larsen, G. Margaritondo, J. E. Rowe, M. Schluter, and N. V. Smith, *Phys. Rev. Lett.* **58**, 423 (1976).
- ⁸P. Thiry, Y. Petroff, R. Pinchaux, C. Guillot, Y. Ballu, J. Lecante, J. Paigné, and F. Levy, *Solid State Commun.* **22**, 685 (1977).
- ⁹J. A. Wilson, F. J. Di Salvo, and S. Mahajan, *Adv. Phys.* **24**, 117 (1975).
- ¹⁰A. M. Woolley and G. Wexler, *J. Phys. C* **10**, 2601 (1977).
- ¹¹R. A. Pollak, D. E. Eastman, F. J. Himpsel, P. Heimann, and B. Reihl, *Phys. Rev. B* **24**, 7435 (1981).
- ¹²D. K. G. de Boer, C. F. van Bruggen, G. W. Bus, R. Coehoorn, C. Haas, G. A. Sawatzky, H. W. Myron, D. Norman, and H. Padmore, *Phys. Rev. B* **29**, 6797 (1984).
- ¹³M. Schärli, J. Brunner, H. P. Vaterhaus, and F. Lévy, *J. Phys. C* **16**, 1527 (1983).
- ¹⁴J. V. McCann, R. H. Williams, R. B. Murray, and P. C. Kemeny, *J. Phys. C* **10**, 4255 (1977).
- ¹⁵G. Lal and G. C. Trigunayat, *J. Solid State Chem.* **9**, 132 (1974).
- ¹⁶J. Bordas, J. Robertson, and A. Jakobsson, *J. Phys. C* **11**, 2607 (1978).
- ¹⁷J. Robertson, *J. Phys. C* **12**, 4753 (1979).
- ¹⁸J. Thomas, I. Pollini, and A. Lenselink (unpublished).
- ¹⁹D. L. Greenaway and G. Harbeke, *Proceedings of the International Conference on Semiconductors, Kyoto, Japan, 1966* [*J. Phys. Soc. Jpn. Suppl.* **21**, 151 (1966)]; D. L. Greenaway and R. Nitsche, *J. Phys. Chem. Solids* **26**, 1445 (1965).
- ²⁰H. Matsumoto, H. Nakagawa, and S. Kondo, *Mem. Fac. Eng. Fukui Univ.* **31**, 53 (1983).
- ²¹R. M. Yu, *J. Phys. Chem. Solids* **30**, 63 (1969).
- ²²D. K. Wright and M. R. Tubbs, *Phys. Status Solidi* **37**, 551 (1970).
- ²³T. Hayashi, T. Ohata, and S. Koshiro, *Solid State Commun.* **38**, 845 (1981).
- ²⁴A. D. Brothers and J. T. Pajor, *Phys. Rev. B* **14**, 4570 (1976).
- ²⁵R. D. Bringans and W. Y. Liang, *J. Phys. C* **14**, 1065 (1981).
- ²⁶G. C. Trigunayat and G. K. Chadha, *Phys. Status Solidi A* **4**, 9 (1971).
- ²⁷R. W. G. Wyckoff, *Crystal Structures*, 2nd ed. (Interscience, New York, 1960), Vol. 1.
- ²⁸A. R. Williams, J. Kübler, and G. D. Gelatt, Jr., *Phys. Rev. B* **19**, 6094 (1979).
- ²⁹L. Hedin and B. I. Lundqvist, *J. Phys. C* **4**, 2064 (1971).
- ³⁰M. Methfessel and J. Kübler, *J. Phys. F* **12**, 141 (1982).
- ³¹C. E. Moore, *Natl. Bur. Stand. (U.S.) Circ. No. 467* (U.S. G.P.O., Washington, D.C., 1949).
- ³²J. C. Phillips, in *Solid State Physics*, edited by F. Seitz, D. Turnbull, and H. Ehrenreich (Academic, New York, 1966), p. 56.
- ³³S. C. Miller and W. F. Love, *Tables of Irreducible Representations of Space Groups and Corepresentations of Magnetic Space Groups* (Pruett, Boulder, 1967).
- ³⁴R. B. Murray, R. A. Bromley, and A. D. Yoffe, *J. Phys. C* **5**, 746 (1972).
- ³⁵L. F. Mattheiss, *Phys. Rev. B* **8**, 3719 (1973).
- ³⁶A. Zunger and M. L. Cohen, *Phys. Rev. B* **18**, 5449 (1978).
- ³⁷J. P. Perdew and A. Zunger, *Phys. Rev. B* **23**, 5048 (1981).
- ³⁸S. Nagel, A. Baldereschi, and K. Maschke, *J. Phys. C* **12**, 1625 (1979).
- ³⁹B. Feuerbacher, B. Fitton, and R. F. Willis, *Photoemission and the Electronic Properties of Surface* (Wiley, New York, 1978).
- ⁴⁰Y. Petroff, *J. Phys. (Paris) Colloq.* **39**, C4-149 (1978).
- ⁴¹N. V. Smith, in *Photoemission in Solids I*, edited by M. Cardona and L. Ley (Springer, Berlin, 1978).
- ⁴²F. J. Himpsel, *Adv. Phys.* **32**, 1 (1983).
- ⁴³N. J. Shevchik and D. Liebowitz, *Phys. Rev. B* **18**, 1618 (1978).
- ⁴⁴J. F. L. Hopkinson, J. B. Pendry, and D. J. Titterton, *Comput. Phys. Commun.* **19**, 69 (1980).
- ⁴⁵A. Liebsch, in *Electron and Ion Spectroscopy of Solids*, edited by L. Fiermans, J. Vennik, and W. de Keyser (Plenum, New York, 1978), p. 93.
- ⁴⁶D. J. Spanjaard, D. W. Jepsen, and P. M. Marcus, *Phys. Rev. B* **15**, 1728 (1977).
- ⁴⁷D. W. Jepsen, F. J. Himpsel, and D. E. Eastman, *Phys. Rev. B* **26**, 4039 (1982).
- ⁴⁸T. Grandke, L. Ley, and M. Cardona, *Phys. Rev. B* **18**, 3847 (1978).
- ⁴⁹F. Minami, M. Sehit, M. Aono, and N. Tsuda, *Solid State Commun.* **29**, 459 (1979).
- ⁵⁰P. E. Fiebleman and D. E. Eastman, *Phys. Rev. B* **10**, 4932 (1974).
- ⁵¹A. Liebsch, *Solid State Commun.* **19**, 1193 (1976).
- ⁵²N. J. Shevchik, *Phys. Rev. B* **20**, 3020 (1979).
- ⁵³J. Hermanson, *Solid State Commun.* **22**, 9 (1977).
- ⁵⁴G. K. Wertheim and D. N. E. Buchanan, *Phys. Rev. B* **16**, 2613 (1977).
- ⁵⁵L. Ley, R. A. Pollak, F. R. McFeeley, S. P. Kwalczyk, and D. A. Shirley, *Phys. Rev. B* **9**, 600 (1974).
- ⁵⁶N. J. Shevchik, J. Tejeda, D. W. Langer, and M. Cardona, *Phys. Status Solidi* **60**, 345 (1973).
- ⁵⁷N. G. Stoffel, *Phys. Rev. B* **28**, 3306 (1983).
- ⁵⁸J. H. Scofield, *J. Electron Spectrosc. Relat. Phenom.* **8**, 129 (1976).
- ⁵⁹S. Doniach and M. Šunjić, *J. Phys. C* **3**, 285 (1970).
- ⁶⁰R. Coehoorn, A. A. van Huizen, C. Haas and G. A. Sawatzky, in *Festkörperprobleme—Advances in Solid State Physics*, (Vieweg, Braunschweig, in press), Vol. XXV.